RSC Advances

PAPER

View Article Online
View Journal | View Issue

Cite this: *RSC Adv.*, 2022, **12**, 21957

PBAT/gelatin hybrid nanofibers based on post-double network bond processing as a promising vascular substitute

Jiakun Nie,†[a] Changjie Jin,†[c] Yonghang Liu,†[c] Juan Du,[c] Sihao Chen,[c] Yujia Zheng*[b] and Binbin Lou *[cd]

The development of injured vascular tissue substitutes with proangiogenic, anti-thrombus, and anti-hyperplasia activity still remains a major challenge in vascular tissue engineering. In this study, we have prepared a series of poly(butylene adipate-*co*-terephthalate)/gelatin hybrid nanofibers (P/G) through random electrospinning and post-double network bond crosslinking for process optimization according to physiochemical and mechanical properties as well as promoting enhanced vascular cell viability *in vitro*. The gelatin matrix was shown to be successfully contained in the bicomponent hybrid P/G nanofibers, and the formed P/G nanofibers exhibited a uniform and smooth morphology. Importantly, the bicomponent hybrid nanofibers showed a potentially reliable ability to promote the proliferation of human umbilical vein endothelial cells (HUVECs). In addition, all the results demonstrated the significantly stable microstructure, appropriate surface wettability, matched mechanical properties, and excellent blood compatibility, cellular compatibility, and histocompatibility of hybrid nanofibers containing 15 wt% gelation (P/G-15) compared to PG-0, P/G-5, and PG-25 groups, indicating their potential for vascular injury healing.

Received 10th April 2022
Accepted 27th July 2022

DOI: 10.1039/d2ra02313j

rsc.li/rsc-advances

1. Introduction

Vascular disease is a condition related to narrowing, blockage or trauma of blood vessels.[1–3] Despite the rapid development of vascular surgical skills and artificial blood vessel replacement in recent years, there is still a problem of poor bioactivity and biocompatibility of artificial blood vessel materials and imperious demands of stable artificial blood vessels.[4–6] At present, the gold standard of vascular transplantation is still derived from autologous arteries or veins.[7–11] However, due to the lack of donors of autologous vascular tissue, anatomical differences and immunogenicity, the clinical application of autologous blood vessels is greatly limited.[12] Therefore, the development of new materials that can be used in artificial blood vessels with proangiogenic, anti-thrombus, and anti-hyperplasia properties after vascular transplantation is still the most promising solution for the treatment of vascular diseases.

Poly(butylene adipate-*co*-terephthalate) (PBAT) is a biodegradable flexible synthetic polyester with high elongation, excellent flexibility and good processability, which makes it suitable as an optional biopolymer for vascular tissue repairing.[13–15] In addition, due to the prominent cytocompatibility of PBAT, a large number of previous studies in recent years have shown that PBAT and its complexes possessed potential uses in the field of biomedicine.[16,17] Alessandro *et al.*[18] reported a polypyrrole-enhanced electrospun hybrid PBAT fiber for promoting branching and neurite extension in Neuro2A cells. The results indicated that this hybrid fibers scaffold containing PBAT, and a conductive polymer (polypyrrole, PPy) presented significant effect for neuronal growth and differentiation. Liu *et al.*[19] proposed and prepared a PBAT-based hollow porous fiber (HPMF), which can be loaded with more polypeptides as well as solved a series of major challenges of drug-loading and controlled release in pharmacy. Ulbrich *et al.*[20] reported a 3D printed PBAT/BAGNb composite scaffold for bone repairing *in vivo*. The relative experimental data *in vivo* showed that PBAT/BAGNb exhibited more obvious new bone formation compared with the positive control group. Whereas, even though PBAT exhibit acceptable biocompatibility, it is still a bioinert synthetic polymer, which is no active site recognized by the host cell on the surface of the molecular chain of PBAT. So, it is necessary to modify PBAT by enhance the biological

[a]*Fuzhou Medical College, Nanchang University, 9 Donglin Rd., Fuzhou 344000, Jiangxi, P. R. China*

[b]*Shanghai Institute of Measurement and Testing Technology, 1500 Zhang Heng Rd., Shanghai 201203, P. R. China*

[c]*School of Chemistry and Chemical Engineering, Shanghai Engineering Research Center of Pharmaceutical Intelligent Equipment, Shanghai Frontiers Science Research Center for Druggability of Cardiovascular Non-coding RNA, Institute for Frontier Medical Technology, Shanghai University of Engineering Science, 333 Longteng Rd., Shanghai 201620, P. R. China. E-mail: binbin.lou@shgh.cn; lewisjia@163.com*

[d]*Department of Stomatology, Shanghai General Hospital, Shanghai Jiao Tong University School of Medicine, 650 Xinsongjiang Rd., Songjiang District, Shanghai 201600, P. R. China*

† These authors contributed equally to this work.

activity. Varshosaz *et al.*[21] reported an RGD-modified PBAT/gelatin nanofiber mat for potential applications in promoting wound healing. The results showed that this above nanofiber mat exhibited the properties of non-cytotoxic, promoted epithelialization and collagen deposition and angiogenesis.

Gelatin is a translucent natural organic polymer. Its unique amino acid sequence endows it with good biological activity, which can maintain cell viability,[22–24] enhance cell adhesion,[25] and promote host cell proliferation.[26] However, the electrospun gelatin fibers mat is relatively brittle,[27] and is easy to tear during suture, which cannot meet the suture requirements of transplant surgery.[28] Therefore, most of the current research on gelatin tissue engineering scaffolds is focused on the preparation of PBAT and gelatin into scaffolds for biomimetic extracellular matrix by synergistic techniques of physical blending/chemical post-processing.[29] The nanofibers mat, which prepared by electrospinning, can realistically simulate the three-dimensional structure of the extracellular matrix.[30,31] This provides an effective strategy for the regeneration of damaged tissue.

Based on the above review, to clarify the synergetic effect of active component content and three-dimensional structure of hybrid fibers for the growth of endothelial cells, the preset constant concentration of gelatin will compound with PBAT, following the hybrid PBAT/gelatin nanofibers will prepare by random electrospinning and post-double network bond crosslinking for exploring the growth effect and mechanism of human umbilical vein endothelial cells. We will evaluate the physicochemical properties, microscopic morphology, and cytocompatibility of hybrid PBAT/gelatin nanofibers, and then detect the activity of promoting cells proliferation.

2. Materials and methods

2.1 Materials

Poly(butylene adipate-*co*-terephthalate) (PBAT, M_w = 100 000), gelatin (Gel, type B from porcine skin) were purchased from Sigma-Aldrich Trading Co., Ltd. (Shanghai, China). 25% glutaraldehyde solution was purchased from Adamas Reagent Co., Ltd. (Shanghai, China). Human umbilical vein endothelial cells (HUVEC) for *in vitro* experiments were obtained from Shanghai Cell Bank of Chinese Academy of Sciences (Shanghai, China). Cell counting kit (CCK-8) was obtained from Sigma-Aldrich Trading Co., Ltd. (Shanghai, China). Dulbecco's modified eagle medium (DMEM), Fetal bovine serum (FBS), and antibiotic-antibacterial medicine (penicillin/streptomycin) were purchased from Hyclone Trading Co., Ltd. (Shanghai, China). Hexafluoroisopropanol (HFIP, purity ≥99.56%) was obtained from Shanghai Darui Fine Chemicals Co., Ltd. (Shanghai, China). Unless otherwise specified, all the above reagents were used directly. All the materials were used as received, except where mentioned otherwise.

2.2 Fabrication of nanofibers mats and nanofibers tubular grafts

PBAT and gelatin were mixed and then dissolved in 10 mL of HFIP at a mass ratio of 100 : 0, 95 : 5, 85 : 15, 75 : 25, forming electrospinning solution with a relative mass fraction $W_{gelatin}/W_{PBAT+gelatin}$ of 0%, 5%, 15%, and 25% under vigorous stirring at room temperature for 72 h, respectively. Then, the 10 mL of the above prepared mixture solution were fed at 1.0 mL h^{-1} from a steel capillary charged at 15 kV to generate nanofibers. The as-electrospun nanofibers were collected onto a flat aluminum foil board located 14 cm from the capillary to form nanofibers mats. Then nanofibers mats were vacuumed in a desiccator for 48 h to remove residual HFIP. Similarly, the aselectrospun nanofibers were collected onto a stainless-steel bar (2 mm diameter, 100 mm length, rotated at 200 rpm) located 14 cm from the capillary to form tubular grafts.

Finally, the above nanofibers mats crosslinked with glutaraldehyde vapor (named P/G-0, P/G-5, P/G-15, and P/G-25, respectively) were also prepared. Crosslinking was carried out by placing samples into 10 mL of a 25% glutaraldehyde solution (aqueous). The nanofibers mats, along with beakers, were kept inside a sealed desiccator and allowed to crosslink with glutaraldehyde vapor for 3 h at room temperature. The crosslinked nanofibers mats were then washed in a 5% glutamic acid solution (1.8% hydrochloric acid as a solvent) and doubly-distilled water, respectively, then dried under reduced pressure prior to use.

2.3 Characterization and testing

The morphology and surface structure of nanofibers mats were carried out using a scanning electron microscope (SEM, Phenom XL, Netherlands) operating with sputter gold plating for 35 s at 5 mA at an accelerating voltage of 10 kV. The diameters of the electrospun nanofibers mats were measured using Image J software ((National Institutes of Health, USA)) on the basis of the SEM images. One hundred fibers diameters on different parts of the SEM images were chosen randomly, thus measuring the distribution of fibers diameters. A contact angle measuring device (JC 2000D 2A, Shanghai Zhongchen Digital Technology Equipment Co., Ltd, China) was used to testing the wettability of nanofibers mats. In this testing, 0.02 mL deionized water was added to the sample and three different positions of the sample were taken to test the water contact angle and calculate the average value. Image-J (National Institutes of Health, USA) was adopted to determine the diameter of nanofibers.

The porosity of the mats was tested *via* the ethanol infiltration method.[32,33] A slice of the mat was immersed in the ethanol; the volume of ethanol in the measuring cylinder before and after the nanofibers mat immersion was set as V_1 and V_2, respectively. After 15 minutes, the mat was removed from the ethanol, and the remaining volume was marked as V_3; the porosity of the tested membranes was calculated according to eqn (1):

$$\text{Porosity}(\%) = \frac{V_1 - V_3}{V_2 - V_3} \times 100\% \quad (1)$$

High-precision tensile testing machine (HY-025CS, Shanghai Hengyu Instrument Co., Ltd, China) with a transducer with a load range of 0–200 N was employed to testing the mechanical

properties of nanofibers mats in wet conditions at room temperature strictly according to ISO 7198:1998. Each sample was cut into a rectangular strip with length × width × thickness = 50 mm × 10 mm × 0.6 mm, then soaked in 0.01 M phosphate buffer (PBS, pH = 6.8) for 24 h. Finally, tensile tests were investigated at room temperature with a stretching speed of 1 mm min^{-1}. The specimens were extended until breaking under tensile force and the tensile stress–strain curves were recorded. Each test was repeated five times during mechanical analysis. The tensile strength, elongation at tensile strength, the representative modulus, and first order equation fitting of stress and strain within the magnification of calculating range were calculated according to the results of stress–strain.

The stress–strain curves, Young's modulus, and cyclic compression curves at 50% deformation of the scaffolds were tested in dry conditions by a tensile and cyclic tensile testing machine (HY-940FS, Shanghai Hengyu Instrument Co., Ltd, China). The tensile tests at a fixed rate of 0.2 mm min^{-1} and the cyclic tensile tests were repeated for 10 cycles at a fixed rate of 0.2 mm min^{-1}.

2.4 Hemolysis test *in vitro*

The detailed experimental procedures of the hemolysis test *in vitro* were followed according to the protocol of GB/T 16886.4-2003 of China. The experimental sample set consisted of P/G-0, P/G-5, P/G-15, and P/G-25 nanofibers mats (3 cm × 1 cm). Milli-Q water served as a positive control and 0.9% normal saline (0.9% NS) acted as a negative control.

2.5 Cell culture *in vitro*

Human umbilical vein endothelial cells (HUVECs) were obtained from Shanghai Cell Bank of Chinese Academy of Sciences (Shanghai, China) and cultured with growth medium consists of Dulbecco's modified eagle medium (DMEM), 10% fetal bovine serum and 1% penicillin/streptomycin. Before cell seeding, the P/G-0, P/G-5, P/G-15, and P/G-25 nanofibers mats were cut into discs with a diameter of 14 mm, then placed into 24-well plates one by one, following covered with sterilized stainless rings, respectively. Each sample was sterilized in 75% ethanol for 12 h and then washed with PBS three times, finally irradiated with ultraviolet for 2 h and socked in growth medium for incubation overnight. HUVECs were seeded at a density of 1.0×10^4 cells per well, and the culture medium was maintained to be replaced every 2 days.

The cell viability of HUVECs were tested by using the cell counting kit-8 (CCK-8). The cells were cultured in P/G-0, P/G-5, P/G-15, and P/G-25 nanofibers mats for 1 day, 4 days, and 7 days, respectively. When the set culture time point, the well plate was taken from the CO_2 incubator, and then a series of operations as removal medium, wash samples in well with PBS, adding 360 μL DMEM medium and 40 μL CCK-8 solution into the lucifugal well plate in sequence. After 4 h incubation in CO_2 incubator, the liquid in the well plate was removed, following added 400 μL of dimethyl sulfoxide (DMSO). Then the above well plate was placed in 37 °C shaker for 30 min. The OD value was measured with a microplate reader at a wavelength of 490 nm.

Then, the proliferous HUVECs were fixed with 4% paraformaldehyde and dehydrated by gradient ethanol (10%, 30%, 50%, 60%, 75%, 80%, 90%, 100%) on the 4th day and the morphology carried out using a scanning electron microscope (SEM, Phenom XL, Netherlands) operating with sputter gold plating for 35 s at 5 mA at an accelerating voltage of 10 kV, respectively.

2.6 *In situ* replacement of rabbit carotid artery

Animal experimental procedures were approved by the Institutional Animal Care and Use Committee of Shanghai General Hospital. Animals were purchased from Shanghai SLAC Laboratory Animal Co., Ltd (Shanghai, China), and all animal experiments were conducted following China's "Regulations on the Administration of Animals" (1988, revised in 2001, Ministry of Science and Technology).

Twelve male New Zealand white rabbits weighing 2.5–3.0 kg (two of the rabbits were used as backup) were selected to establish the unilateral carotid artery's replacement models. A 10 mm long defect in the left carotid artery was replaced with P/G-15 (2 mm in inner diameter, 10 mm in length, and approximately 0.16 mm in wall thickness), which was then sutured end-to-end to the carotid artery. Performance of P/G-15 was evaluated after surgery for two and four weeks, respectively.

Two and four weeks after transplantation, rats and rabbits were anesthetized with pentobarbital, and images were acquired using a Doppler ultrasound platform (GE LOGIQ 9, GE Medical Systems, USA) to assess rabbits' vascular function. The implanted tubular grafts were removed, and histological analysis of the grafts was performed. The detail as: Samples were processed, sectioned to 5 μm thickness and stained with hematoxylin and eosin (H&E) staining and Masson's trichrome staining for histological analysis. The slides were observed using a light microscope (Olympus BX41, Japan) and photographed by DP71 camera (Olympus, Japan). For immunofluorescent staining. The nuclei were counterstained with DAPI containing mounting solution (Dapi Fluoromount G, Southern Biotech, England). The smooth muscle cells were stained using rabbit anti-α-SMA (α-SMA, Boster, China).

2.7 Statistical analysis

The respective experiment was repeated three times, and the data were expressed as mean ± standard deviation. The data here were analyzed by conducting the single factorial analysis. When p was lower than 0.05, the difference was significant (*); $0.01 < p < 0.05$, the difference was very significant (**).

3. Results and discussion

Although the research on vascular materials has made breakthrough progress and shown promising prospects in clinical trials.[34] However, there is no relevant literature reporting clinical trials related to small-diameter tissue-engineered blood vessels. The clinical application of tissue-engineered blood vessels still faces many challenges.[35] In particular, these natural or synthetic derived vascular materials are likely to cause

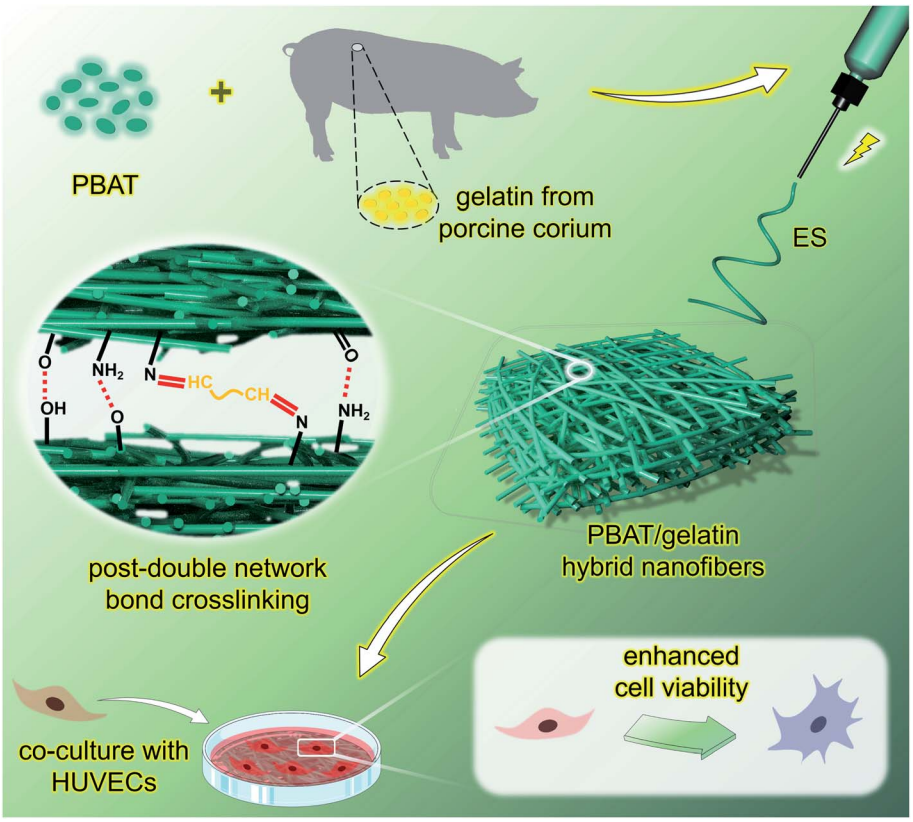

Fig. 1 Schematic illustration of the preparation for the PBAT/gelatin hybrid nanofibers by random electrospinning and post-double network bond crosslinking (Schiff based reaction, and hydrogen-bonding network densification) and its effective enhanced cell viability co-culture with HUVECs.

antigen–antibody immune rejection when implanted into the body. On the other hand, the biomechanical properties and degradation properties of synthetic polymer vascular materials can be controlled and customized, although their compatibility is poor.[36] In short, composite materials with natural active components, mechanically guaranteed and controllable degradation properties are the prefs for the manufacture of artificial blood vessels.

Electrospun nanofibers have the advantages of high specific surface area, high porosity, small size and surface effect, and the three-dimensional structure similar to the extracellular matrix,[27,37–40] which can be used for the adhesion, proliferation, growth and differentiation of host cells *in vitro* or *in vivo* as well as provide an ideal microenvironment for intercellular communication.[41,42] Moreover, the high-performing composite nanofibers can be prepared using natural polymer materials with good bioactivity and synthetic polymer materials with good mechanical properties *via* electrospinning, which provides a facile method for the preparation of nanofiber scaffolds with good bioactivity and functionality.[43,44] However, there are still many problems and challenges in how to better control the microstructure, mechanical properties and functions of composite nanofibers.

So, we believe that the optimal screening of composite nanofibers is a very important according to the aggregative indicator as physicochemical properties, microscopic morphology, and cytocompatibility, *et al.* Based on the above considerations, we have designed and prepared a series of poly(butylene adipate-*co*-terephthalate)/gelatin hybrid nanofibers (P/G) through random electrospinning and post-double network bond crosslinking for process optimization according to physiochemical and mechanical properties as well as promoting enhanced vascular cells viability *in vitro* (Fig. 1).

3.1 Morphology, microstructure, and surface wettability

Suitable vascular materials should have appropriate porosity, larger specific surface area, and suitable surface wettability properties.[45] PBAT/gelatin composites could be feasibly dissolved in HFIP to form a uniform solution for electrospinning and collected by a rotating steel bar (Fig. 1A) to obtain a nanofibers tubular graft (Fig. 1B and C). Macroscopically, the graft could maintain its tubular shape (Fig. 1C) after being peeled from the steel bar. We obtained tubular grafts with a length of 30 mm and an inner diameter of 1.8 mm (Fig. 1C). Cross-section images showed that the tubular graft has a thick wall (approximately 500 μm) composed of densely compacted nanofibers (Fig. 1C), indicating it might effectively withstand the blood flow without leakage.

The scanning electron microscope images in Fig. 2D showed that the orientation of the nanofibers was random and the

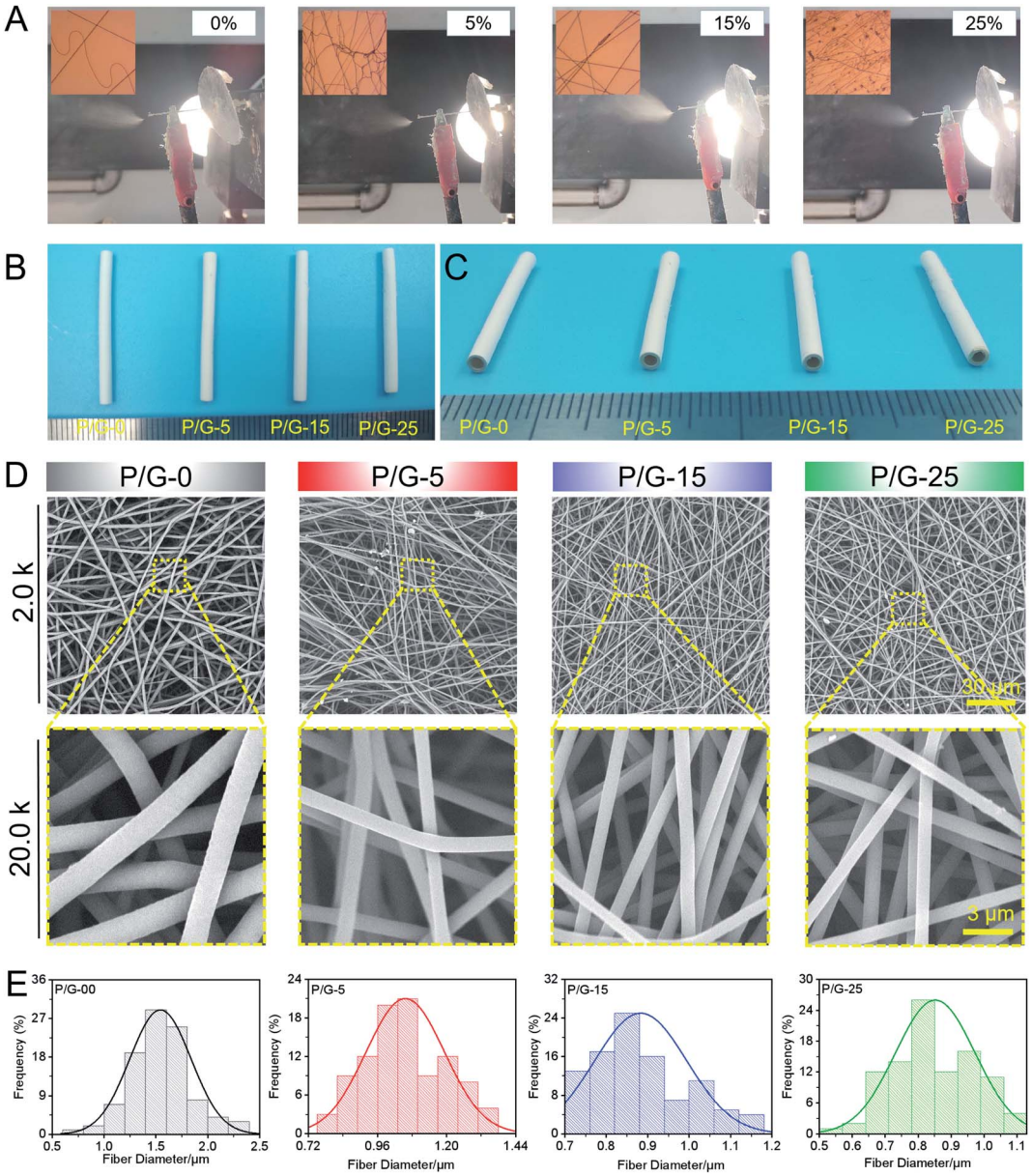

Fig. 2 (A) The digital photos of P/G-0, P/G-5, P/G-15, and P/G-25 fibers *via* electrospinning, inset: metallographic photomicrograph; (B) and (C) appearance images of outer surface and cross section of P/G-0, P/G-5, P/G-15, and P/G-25, respectively; (D) SEM images and (E) fiber diameter distribution histograms of P/G-0, P/G-5, P/G-15, and P/G-25, respectively.

surface was uniform, smooth and without beading and agglomeration. The diameter distribution of each group of nanofibers was different (Table 1). The statistical datas of diameter showed that the average diameter of P/G-0, P/G-5, P/G-15, and P/G-25 groups were 1.54 ± 0.12, 1.06 ± 0.17, 0.88 ± 0.19 and 0.85 ± 0.16 μm (Fig. 1E). The diameter of P/G-0 group was coarse but evenly distributed. However, we also found that the average diameter decreased from 1.54 to 0.85 μm ($P < 0.001$) as the content of gelatin in the fiber component increases (Table 1). The above phenomenon was attributed to the fact that the

Table 1 Mean diameter and standard deviation of P/G-0, P/G-5, P/G-15, and P/G-25 fibers, respectively (data are representatives of independent experiments and all data are given as mean ± SD, $n = 5$)

Samples	P/G-0	P/G-5	P/G-15	P/G-25
Mean diameter (μm)	1.54 ± 0.12	1.06 ± 0.17	0.88 ± 0.19	0.85 ± 0.16
Standard deviation (μm)	0.30 ± 0.04	0.14 ± 0.06	0.11 ± 0.07	0.12 ± 0.05

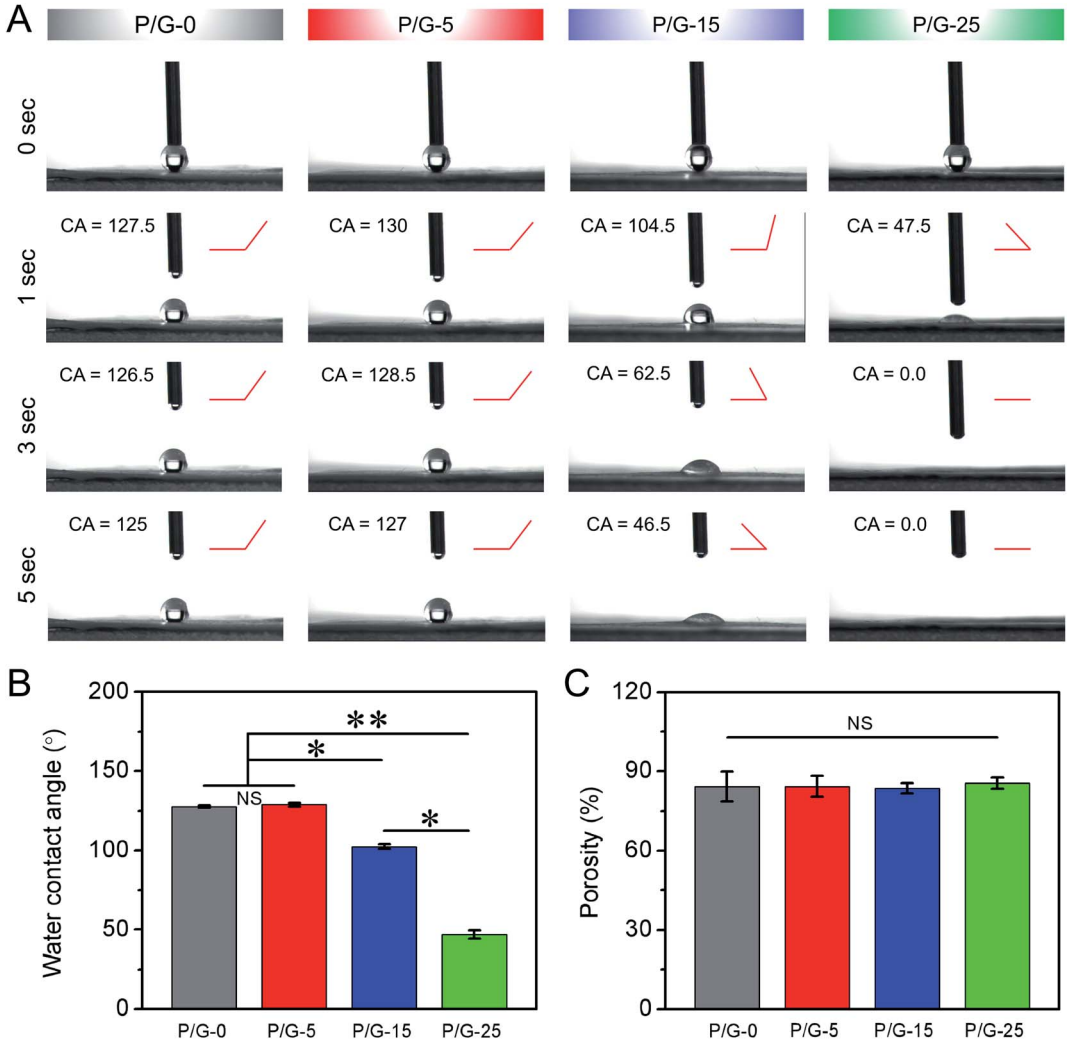

Fig. 3 (A) Captured images of dynamic water contact angle of P/G-0, P/G-5, P/G-15, and P/G-25 at the 1, 3, and 5 seconds time point, respectively; (B) water contact angle of P/G-0, P/G-5, P/G-15, and P/G-25 at the 1 second time point, respectively; (C) porosity of P/G-0, P/G-5, P/G-15, and P/G-25, respectively. (NS: not significant, $*p < 0.05$, $**p < 0.01$, $n = 5$).

electric charge carried by gelatin increases the electric field force of the spinning solution at the needle, resulting in the nanofibers with smaller diameter.

The wettability properties of the surface of nanofibers mats play an important role in the adsorption of proteins and the adhesion of cells. Many prior studies have shown that a moderately hydrophilic surface is easier to promote cell adhesion, growth and proliferation.[46] As shown in Fig. 3A and B, the water contact angle values of P/G-0, P/G-5, P/G-15, and P/G-25 were 127.5°, 130.0°, 104.5° and 47.5° at 1 second, respectively. The water contact angle values decreased with the increase of gelatin from 5 wt% to 25 wt%, indicating that more components of gelatin could furtherly improve the hydrophilicity of P/G nanofibers mats. In addition, we also found that the water contact angle in P/G-5 group was consistently greater than that in P/G-0 group, regardless of the time point. This may due to the smaller fibers diameter and the higher porosity of P/G-5 than P/G-0 (Fig. 3C). Moreover, the large fiber diameter, which along with large pore size, will enhance the infiltration of PBS solution into the nanofibers, which accelerating the infiltration of solution. In short, the wettability properties of nanofibers mats are closely related to the microscopic morphology and constituent content of the nanofibers in mat, as well as a huge impact on host cell growth. And the wettability and structure of the material surface plays an indispensable role in the adsorption properties of the protein, which secreted from the host cell.

3.2 Mechanical properties of nanofibers mats

For the growth of vascular cell and vascular tissue regeneration, the mechanical property of grafts plays an important role.[47] Nanofibers grafts will be subject to the stress of the tissue around the injured blood vessel, such as blood pressure, human traction, *etc.*, when used for vascular repairing. Therefore, the designed and optimized nanofibers should exhibit a matched mechanical property with autogenous tissue to support tissue regeneration.[40] We have finished the mechanical properties of nanofibers mats in wet conditions at room temperature strictly

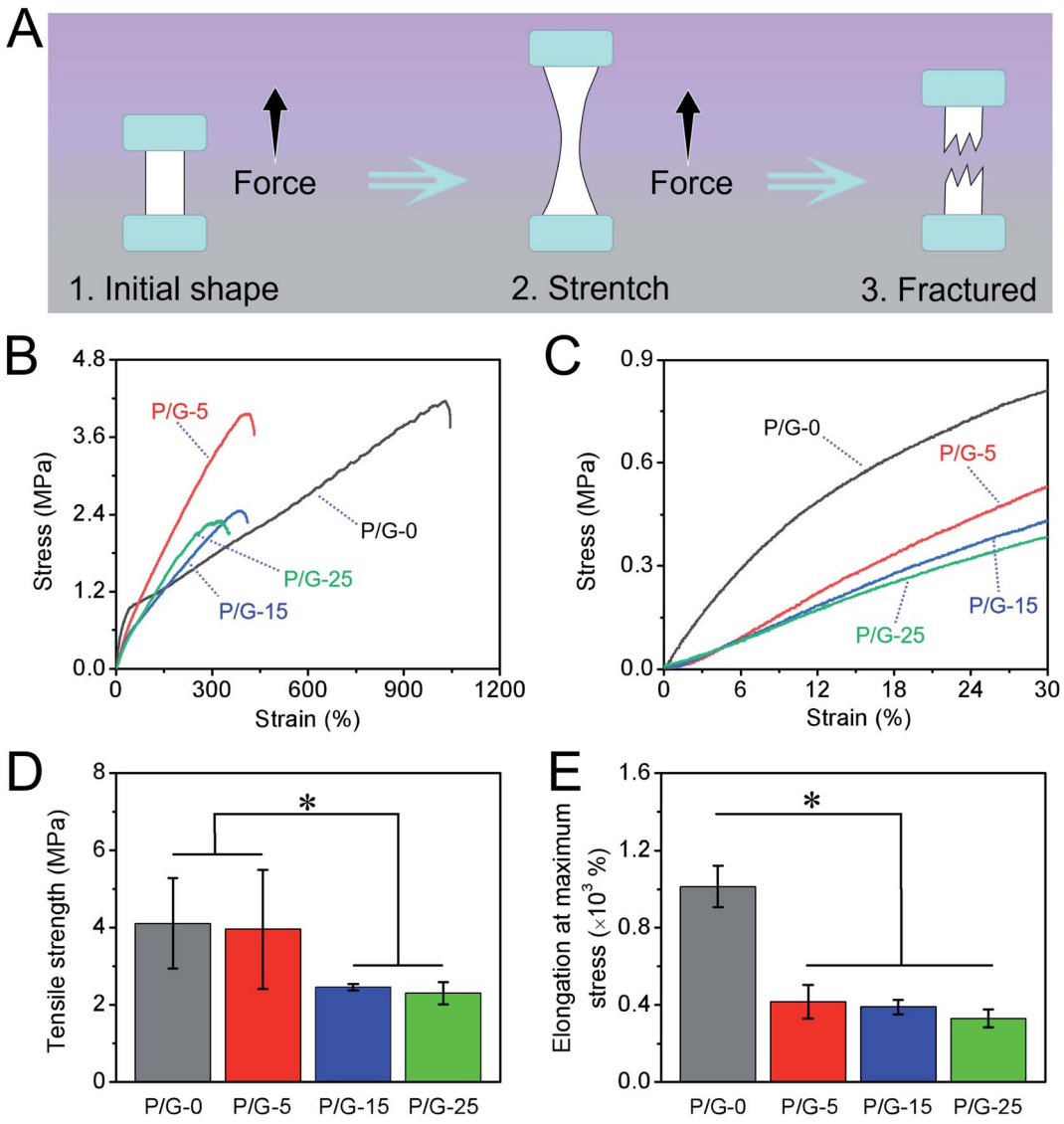

Fig. 4 Mechanical properties of prepared nanofibers mats under dry conditions. (A) Schematic illustration of initial shape and fractured shape of nanofibers mats; (B) representative stress–strain curves; (C) the magnification of calculating range of 0–30% modulus; (C) tensile strength; (D) elongation at maximum stress (data are representatives of independent experiments and all data are given as mean ± SD, $*p < 0.05$, $n = 5$).

Table 2 Representative 0–30% modulus of P/G-0, P/G-5, P/G-15, and P/G-25 fibers, respectively (data are representatives of independent experiments and all data are given as mean ± SD, $n = 5$)

Samples	P/G-0	P/G-5	P/G-15	P/G-25
Modulus within 30% (MPa)	3.84 ± 0.03	1.79 ± 0.07	1.49 ± 0.05	1.33 ± 0.06

according to ISO 7198:1998 using the uniaxial high-precision tensile testing machine as the schematic illustration in Fig. 4A. Fig. 4B shows the corresponding representative strain–stress curves of P/G-0, P/G-5, P/G-15, and P/G-25. All nanofibers mats hybridized with gelatin (P/G-5, P/G-15, and P/G-25) showed the typical stress–strain behavior of a linear elastic region in entire stretch zone and deformation before breaking, while the stretching in initial stage of P/G-0 shows elastic mechanical behavior, in which the stress increases sharply with the strain. When the strain starts to enter plastic deformation from 45%, the stress increases slowly with the strain until fracture (Table 2).

3.3 Hemocompatibility and cytocompatibility

Hemocompatibility is an important evaluation index for vascular-related tissue engineering materials. Generally, most of polymers have large non-polar surfaces, low surface energy and hydrophobicity, which are prone to cause adverse reactions such as coagulation, hemolysis, and inflammation after contacting with blood.[48] Therefore, the exploration of blood compatibility of

polymer materials has become the key to solving the problem. The first priority, which need to be solved, is the hemolysis of red cells. When the material comes into contact with blood, hemolysis is induced mainly through three pathways. The first is the mechanical damage of the cell membrane, which caused by the rough surface of the material. The second is that the chemical toxicity from the material will damage red blood cells. Finally, the material matrix can cause oxidative, which damaged the cell membrane and caused cell apoptosis or death. Hemolysis is a phenomenon in which red blood cells are deformed, ruptured, and leaching of hemoglobin and cytoplasm into plasma, which also caused by the damage of cell membrane and oxidation of hemoglobin essentially.

So far, there is no clear consensus on the effect of fiber diameter and microtopography on hemocompatibility. Dong *et al.*[49] found that the smooth surface greatly reduced platelet adhesion and activation compared with nanofibers and microfibers, while promoting the adhesion, spreading, proliferation,

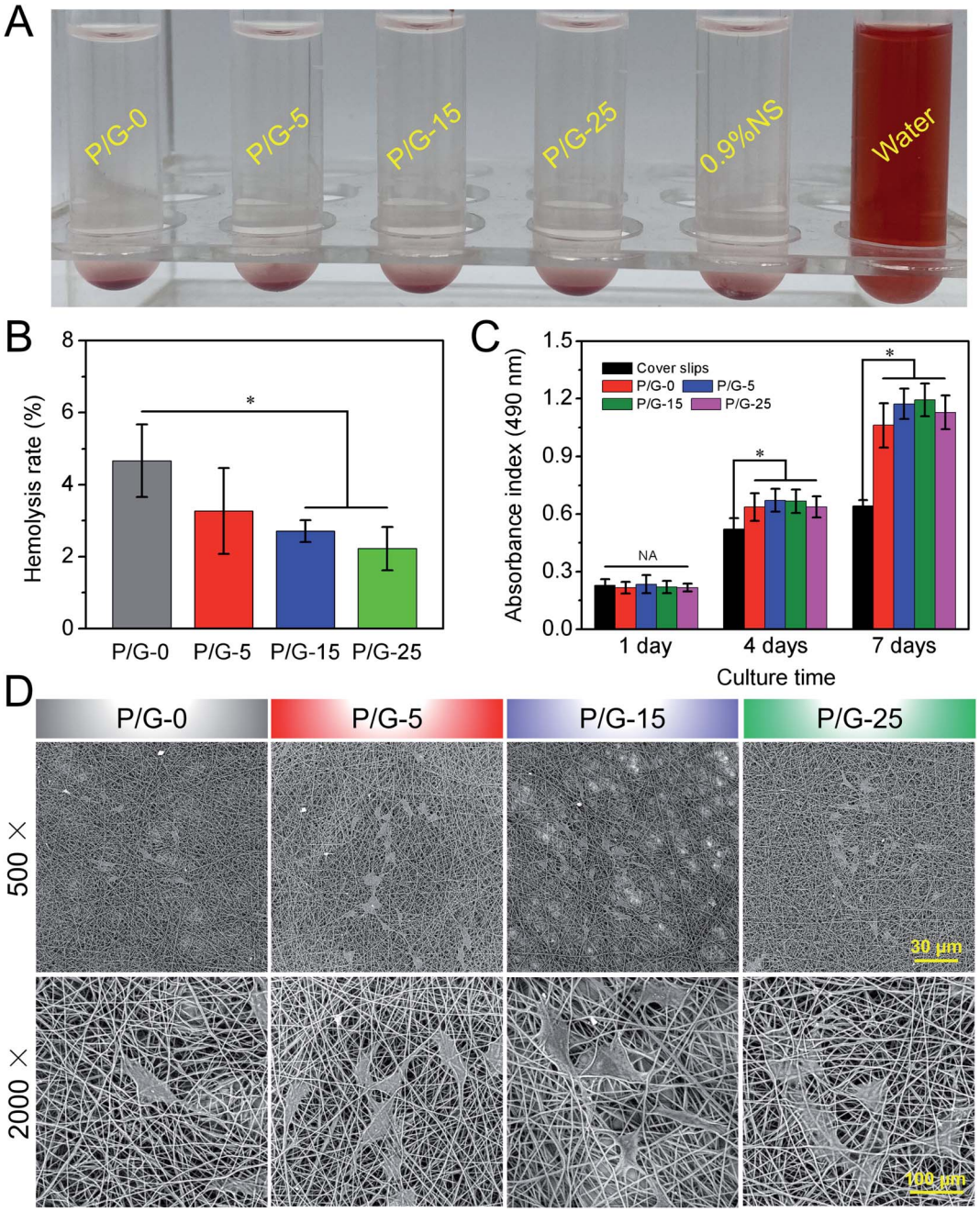

Fig. 5 (A)The photos of supernatant and solution of HRBCs treated with P/G-0, P/G-5, P/G-15, P/G-25, 0.9% normal saline (NS), and water, followed by centrifugation, respectively; (B) the quantification of relative hemolysis rate (HR) of P/G-0, P/G-5, P/G-15, and P/G-25; (C) proliferation viability of HUVECs after culturing for 1, 4, and 7 days on the surface of P/G-0, P/G-5, P/G-15, and P/G-25, respectively; (D) SEM images of HUVECs on the surface of P/G-0, P/G-5, P/G-15, and P/G-25 after culturing for 4 days. (For hemolysis test, water and 0.9% NS serve as positive and negative groups, respectively; *$p < 0.05$ and NS: not significant, $n = 5$).

migration, and functional expression of endothelial progenitor cells (ECs). As the results in Fig. 5A and B, the hemolysis rate of P/G-0, P/G-5, P/G-15, P/G-25, 0.9% normal saline (NS) (negative control), and water (positive control) were evaluated according to the ISO10993-4 standard, respectively. According to the ISO10993-4 criteria (5%) for blood-contacting biomaterials, these nanofibers can be considered as nonhemolytic and might be safe for the potential application in blood vessel implantation. At the same time, we can also find that with the increase of the gelatin content in the fibers, the hemolysis rate of the nanofibers gradually decreases from P/G-0 to P/G-25. We believe this is mainly due to smaller fiber diameter and less polar charge with increasing gelatin content. The smaller fiber diameter brings the topography of the fiber mat closer to that of a smooth surface. The more gelatin content in the fiber makes the polar charge in the PBAT molecule neutralized by post-double network bond crosslinking.

As we known, microfibers/nanofibers can provide a matrix for cell adhesion and proliferation mainly due to its three-dimensional structure of bionic extracellular matrix and natural cell recognition sites.[50] Here, we have investigated the cell proliferation ability of HUVECs on P/G-0, P/G-5, P/G-15, and P/G-25, respectively. Although the PBAT/gelatin hybrid nanofibers mats could significantly improved the mechanical properties and enhanced stability of three-dimensional structures, the cytotoxicity of the scaffolds was also increased due to the post-double network bond processing. Some prior reports have also confirmed that the residual agent in the mats has certain cytotoxicity to the cell growth. Fig. 5C and D compares the proliferation of HUVECs on nanofibers mats and cover slips, respectively. Compared with synthetic PBAT, nanofibers containing gelatin are more favorable for cell proliferation and differentiation. It is not difficult to find from Fig. 5C that the addition of gelatin can stimulate the growth of endothelial cells. We can also observe that after 7 days of culture for P/G-15 group, the absorbance has approached 1.2, which is the highest value among all groups. Moreover, combining with the SEM images of HUVECs on the surface of P/G-0, P/G-5, P/G-15, and P/G-25 after culturing for 4 days in Fig. 5D, it is not difficult to find HUVECs spreaded significantly on both P/G-15 and P/G-25. The number of HUVECs cultured on P/G-15 reached over that of the other three groups, which might be explained as P/G-15 presented matched microstructure and surface wettability as well as achieved more active site for cell growth.

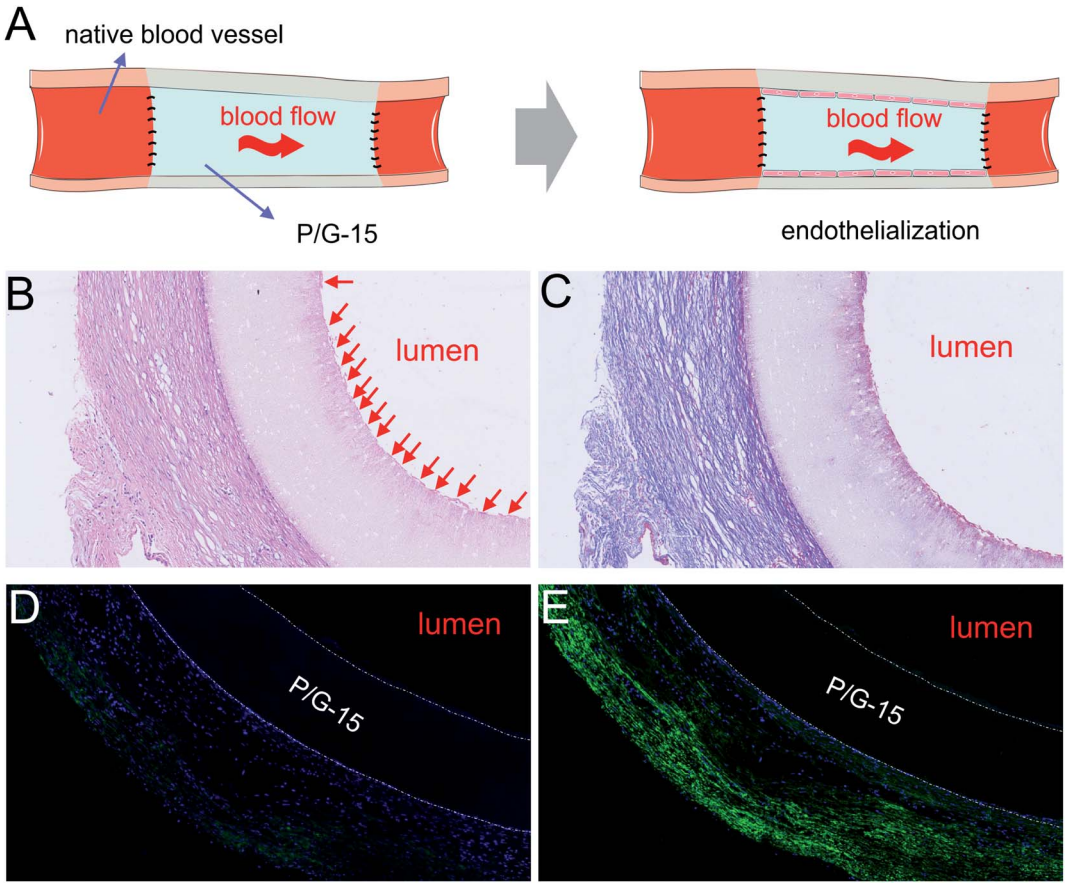

Fig. 6 (A) Schematic illustration for end-to-end anastomosis procedure of the P/G-15 tubular graft suturing to the rabbit's carotid artery and promoting endothelialization; (B) H&E staining of transverse sections of P/G-15 tubular grafts four weeks after surgery; (C) Masson's trichromatic staining of transverse sections of P/G-15 tubular grafts four weeks after surgery. (D) and (E) Immunofluorescent staining of α-SMA positive cells in transverse sections of P/G-15 tubular grafts in midportion after two and four weeks postoperatively, respectively. (Red arrows points to the endothelial cell; cell nuclei were stained with DAPI in blue).

3.4 Patency and regeneration *in vivo*

We prepared electrospun grafts and, followed by replacing isometric left carotid arteries of rabbits with optimized P/G-15 tubular grafts by end-to-end anastomosis (Fig. 6A). No bleeding, leakage, or aneurysm-like expansion at the implantation sites was found. Both H&E (Fig. 6B) and Masson's trichrome (Fig. 6C) staining showed that the P/G-15 tubular graft induced no stenosis or thrombosis up to 4 WEEKs. The P/G-15 tubular graft maintained its original shape and retained vessel wall intact without fibrous loosening or delamination (Fig. 6B and C). Increased hyperplasia and nuclei surrounding the periphery of P/G-15 tubular grafts were observed after four weeks implantation. The suspected endothelial cellular layer covering the lumen were emerged (as all the red arrow pointing to location in Fig. 6B), but no significant proliferation of cells or thrombosis occurred.

Cross-sections of P/G-15 tubular graft in midportion after two and four weeks of implantation were stained against α-SMA (Fig. 6D and E) antibodies and immunofluorescent imaged to demonstrate the presence of smooth muscle cells, respectively. With the increase of transplantation time, the positive expression of smooth muscle cells was more obvious in the periphery of P/G-15 tubular graft, while there was no proliferating smooth muscle tissue in the lumen of P/G-15 tubular graft. No thrombosis occurred within the lumen of grafts after four weeks. Taken together, these data indicated that P/G-15 may be a potential substitute for replacing injured blood vessels.

4. Conclusions

In this study, a series of PBAT/gelatin hybrid nanofibers and nanofibers mats were developed by post-double network bond processing. Subsequently, the diameter size and hydrophilia of the hybrid nanofibers can been regulated by altering the raw material composition and post-processing parameter. Furthermore, these prepared hybrid nanofibers mats exhibited an interconnected pore structure. The hydrophilia of nanofibers mats containing gelatin increased with the addition of gelatin. The hybrid nanofibers mats possessed a controllable mechanical matching property. Both *in vitro* cell experiments and *in situ* replacement of the rabbit carotid artery proved that the optimized PBAT/gelatin hybrid nanofibers, which containing 15 wt% gelatin, exhibited well biocompatibility and maintained patency without acute thrombosis formation. The mentioned result suggested that the P/G-15 available for injured vascular healing.

Conflicts of interest

The authors declare no competing financial interest.

Acknowledgements

The authors sincerely appreciate projects sponsored by National Natural Science Foundation of China (81902186), Shanghai Rising-Star Program (20QC1401300), Science and Technology Commission of Shanghai Municipality (22S31904700, 19441901700, 19441901701, 19441901702), and Construction Project of Shanghai Engineering Technology Research Center (20DZ2255900).

References

1 C. L. Miller, A. R. Kontorovich, K. Hao, L. J. Ma, C. Lyegbe, J. L. M. Bjorkegren and J. C. Kovacic, *J. Am. Coll. Cardiol.*, 2021, **77**, 2531–2550.
2 R. L. Harper, E. A. Ferrante and M. Boehm, *Semin. Immunopathol.*, 2022, **44**(3), 259–268.
3 Y. Luan, K. D. Ren, Y. Luan, X. Chen and Y. Yang, *Front. Cardiovasc. Med.*, 2021, **8**, 770574.
4 W. Duan, Y. Jin, Y. X. Cui, F. N. Xi, X. Y. Liu, F. J. Wo and J. M. Wu, *Biomaterials*, 2021, **272**, 120772.
5 S. M. Nasr, N. Rabiee, S. Hajebi, S. Ahmadi, Y. Fatahi, M. Hosseini, M. Bagherzadeh, A. M. Ghadiri, M. Rabiee, V. Jajarmi and T. Webster, *Int. J. Nanomed.*, 2020, **15**, 4205–4224.
6 S. Bandis, F. Nehl, S. C. Ligon, A. Nigisch, H. Bergmeister, D. Bernhard, J. Stampfl and R. Liska, *Biomed. Mater.*, 2011, **6**, 055033.
7 A. Mahara, S. Somekawa, N. Kobayashi, Y. Hirano, Y. Kimura, T. Fujisato and T. Yamaoka, *Biomaterials*, 2015, **58**, 54–62.
8 F. Askari, A. Solouk, M. Shafieian and A. M. Seifalian, *Artif. Cell Nanomed. Biotechnol.*, 2017, **45**, 999–1010.
9 G. Cittadella, A. de Mel, R. Dee, P. De Coppi and A. M. Seifalian, *Artif. Organs*, 2013, **37**, 423–434.
10 J. Chung and G. P. Clagett, *Semin. Vasc. Surg.*, 2011, **24**, 220–226.
11 T. H. Zhu, H. B. Gu, H. M. Zhang, H. S. Wang, H. T. Xia, X. M. Mo and J. L. Wu, *Acta Biomater.*, 2021, **119**, 211–224.
12 X. Q. Cong, S. M. Zhang, L. Batty and J. Luo, *Stem Cell. Dev.*, 2019, **28**, 1581–1594.
13 M. Dammak, Y. Fourati, Q. Tarrés, M. Delgado-Aguilar and S. Boufi, *Ind. Crop. Prod.*, 2020, **144**, 112061.
14 S. Su, *Mater. Res. Express*, 2022, **9**, 025308.
15 A. Boonprasertpoh, D. Pentrakoon and J. Junkasem, *Cell. Polym.*, 2020, **39**, 31–41.
16 W. C. Jao, C. H. Lin, J. Y. Hsieh, Y. H. Yeh, C. Y. Liu and M. C. Yang, *Polym. Adv. Technol.*, 2010, **21**, 543–553.
17 B. V. M. Rodrigues, A. S. Silva, G. F. S. Melo, L. M. R. Vasconscellos, F. R. Marciano and A. O. Lobo, *Mater. Sci. Eng. C*, 2016, **59**, 782–791.
18 A. E. C. Granato, A. C. Ribeiro, F. R. Marciano, B. V. M. Rodrigues, A. O. Lobo and M. Porcionatto, *Nanomed. Nanotechnol.*, 2018, **14**, 1753–1763.
19 Y. F. Liu, L. Yang, G. J. Chen, Z. T. Liu, T. Lu, Y. Yang, J. Yu, D. D. Kang, W. Yan, M. He, S. H. Qin, J. Yu, C. A. Ye and H. Luo, *Mater. Des.*, 2021, **207**, 109880.
20 L. M. Ulbrich, G. D. Balbinot, G. L. Brotto, V. C. B. Leitune, R. M. D. Soares, F. M. Collares and D. Ponzoni, *J. Tissue Eng. Regener. Med.*, 2022, **16**(3), 267–278.
21 J. Varshosaz, K. Arabloo, N. Sarrami, E. Ghassami, E. Y. Kachouei, M. Kouhi and A. Jahanian-Najafabadi, *Drug Dev. Ind. Pharm.*, 2020, **46**, 484–497.

22 Y. F. Li, C. X. Cao, Y. Pei, X. Y. Liu and K. Y. Tang, *Int. J. Biol. Macromol.*, 2019, **130**, 715–719.
23 H. L. Bai, B. A. Xie, M. X. Li, P. Sun, S. B. Wei, L. W. Zhang and C. Zhang, *Microvasc Res*, 2022, **141**, 104314.
24 D. Hajzamani, P. Shokrollahi, N. Najmoddin and F. Shokrolahi, *Polym. Adv. Technol.*, 2020, **31**, 1896–1910.
25 R. J. Gonzalez-Paz, G. Lligadas, J. C. Ronda, M. Galia, A. M. Ferreira, F. Boccafoschi, G. Ciardelli and V. Cadiz, *J. Biomed. Mater. Res.*, 2013, **101**, 1036–1046.
26 S. T. Koshy, T. C. Ferrante, S. A. Lewin and D. J. Mooney, *Biomaterials*, 2014, **35**, 2477–2487.
27 S. Guessasma and M. Oyen, *Soft Matter*, 2016, **12**, 602–613.
28 Y. Elsayed, C. Lekakou, F. Labeed and P. Tomlins, *Mater. Sci. Eng. C*, 2016, **61**, 473–483.
29 S. Gautam, A. K. Dinda and N. C. Mishra, *J. Mater. Sci.*, 2013, **33**, 1228–1235.
30 S. L. M. Alexander and L. T. J. Korley, *Soft Matter*, 2017, **13**, 283–291.
31 X. R. Xie, Y. J. Chen, X. Y. Wang, X. Q. Xu, Y. H. Shen, A. U. R. Khan, A. Aldalbahi, A. E. Fetz, G. L. Bowlin, M. El-Newehy and X. M. Mo, *J. Mater. Sci. Technol.*, 2020, **59**, 243–261.
32 K. H. Zhang, H. S. Wang, C. Huang, Y. Su, X. M. Mo and Y. Ikada, *J. Biomed. Mater. Res.*, 2010, **93**, 984–993.
33 K. Yu, X. X. Zhou, T. H. Zhu, T. Wu, J. Wang, J. Fang, M. R. El-Assar, H. El-Hamshary, M. El-Newehy and X. M. Mo, *RSC Adv.*, 2016, **6**, 73636–73644.
34 C. D. Devillard and C. A. Marquette, *Front. Bioeng. Biotechnol.*, 2021, **9**, 721843.
35 Y. Zhuang, C. L. Zhang, M. J. Cheng, J. Y. Huang, Q. C. Liu, G. Y. Yuan, K. L. Lin and H. B. Yu, *Bioact. Mater.*, 2021, **6**, 1791–1809.
36 S. Bai, X. Y. Zhang, L. L. Zang, S. Z. Yang, X. Q. Chen and X. Y. Yuan, *Chem. Res. Chin. Univ.*, 2021, **37**, 394–403.
37 H. F. Liu, X. L. Ding, G. Zhou, P. Li, X. Wei and Y. B. Fan, *J. Nanomater.*, 2013, **2013**, 495708.
38 H. L. Zhong, J. Huang, J. Wu and J. H. Du, *Nano Res.*, 2022, **15**, 787–804.
39 S. H. Jiang, Y. M. Chen, G. G. Duan, C. T. Mei, A. Greiner and S. Agarwal, *Polym. Chem.*, 2018, **9**, 2685–2720.
40 J. J. Zhu, D. Chen, J. Du, X. X. Chen, J. H. Wang, H. B. Zhang, S. H. Chen, J. L. Wu, T. H. Zhu and X. M. Mo, *Compos. B Eng.*, 2020, **186**, 107788.
41 Y. Qi, H. Y. Zhai, Y. N. Sun, H. X. Xu, S. H. Wu and S. J. Chen, *Text. Res. J.*, 2021, **92**(9–10), 1537–1549.
42 Z. Mohammadalizadeh, E. Bahremandi-Toloue and S. Karbasi, *J. Mater. Sci.*, 2022, **57**, 4020–4079.
43 J. M. Sharpe, H. Lee, A. R. Hall, K. Bonin and M. Guthold, *Nanomaterials*, 2020, **10**, 1843.
44 J. A. Kluge and R. L. Mauck, in *Advances in Polymer Science, Biomedical Applications of Polymeric Nanofibers*, Springer-Verlag Berlin, Heidelberger Platz 3, D-14197 Berlin, Germany, 2012, vol. 246, pp. 101–130.
45 A. Weekes, N. Bartnikowski, N. Pinto, J. Jenkins, C. Meinert and T. J. Klein, *Acta Biomater.*, 2022, **138**, 92–111.
46 H. Y. Wang, Y. K. Feng, Z. C. Fang, R. F. Xiao, W. J. Yuan and M. Khan, *Macromol. Res.*, 2013, **21**, 860–869.
47 T. H. Zhu, H. B. Gu, W. X. Ma, Q. L. Zhang, J. Du, S. H. Chen, L. M. Wang and W. X. Zhang, *Compos. B Eng.*, 2021, **225**, 109274.
48 J. Zhao and Y. K. Feng, *Adv. Healthc. Mater.*, 2020, **9**, 2000920.
49 X. H. Dong, X. Y. Yuan, L. N. Wang, J. L. Liu, A. C. Midgley, Z. H. Wang, K. Wang, J. F. Liu, M. F. Zhu and D. L. Kong, *Biomaterials*, 2018, **181**, 1–14.
50 Y. D. Han, X. F. Shen, S. H. Chen, X. H. Wang, J. Du and T. H. Zhu, *Front. Chem.*, 2021, **9**, 740191.